ACS OMEGA

Open Access

http://pubs.acs.org/journal/acsodf

Article

Quantum Chemical and Experimental Evaluation of a 4-Amino-Antipyrine Based Schiff Base as Corrosion Inhibitor for Steel Material

Ashwini Narayanswamy, Dileep Ramakrishna, P. V. Raja Shekar, Shashanka Rajendrachari,* and Ranganatha Sudhakar*

Cite This: *ACS Omega* 2024, 9, 13262−13273

Read Online

ACCESS | Metrics & More | Article Recommendations | Supporting Information

ABSTRACT: Electrochemical experiments such as potentiodynamic polarization, electrochemical impedance spectroscopy, and gravimetric studies have been used to examine the corrosion inhibitory efficacy of 4-[(4-nitrobenzylidene)-amino]-antipyrine (4-NBAAP) on mild steel (MS) in 1 M HCl. 4-NBAAP inhibits the corrosion of MS through a mixed inhibition mechanism, according to the electrochemical investigation. The efficiency of 4-NBAAP increases with an increase in the inhibitor concentration and decreases with an increase in temperature. The adsorption of 4-NBAAP molecules on the MS surface follows the Langmuir adsorption isotherm. To find the relationship between the 4-NBAAP molecular structure and inhibitive effect, a few thermodynamic parameters were computed. The experimental results obtained from gravimetric and different electrochemical investigations prove the superiority of the inhibitor at higher concentrations in controlling the corrosion process of the steel in aggressive environments. Also, quantum chemical studies were performed to provide further insights into the inhibition mechanism.

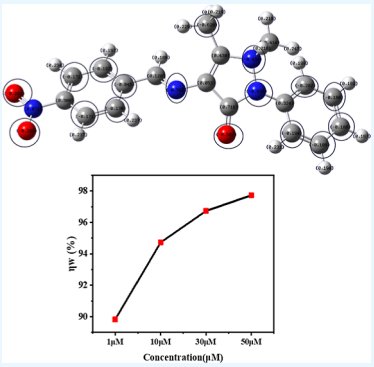

1. INTRODUCTION

The iron alloy of great industrial importance, mild steel (MS), is prone to get corroded in acidic environments due to thermodynamic instability. Despite the tendency to react readily with its environment, MS finds extensive applications in industrial establishments and machineries, as it is economically cheap and has superior mechanical properties. Keeping this in mind, the scientific community has developed various corrosion control strategies, and the one which is effective in reducing the corrosion rates is introducing inhibitor molecules to the aqueous corrosive media. Industrially applied inhibitors are mostly the organic molecules having hetero atoms that enhance their performance in protecting the metal surface from corrosion if the moiety possesses different functional groups, electron densities at donor atoms, and aromaticities. These kinds of features in the molecules support the adsorption on the MS surface to be protected.[1−4]

The condensation process between amines and carbonyl compounds produces Schiff bases, which have been shown to provide excellent corrosion prevention. Also, as the synthetic procedure is simple to carry out with cheap reactants, Schiff bases have become an attractive choice for industrial applications. These compounds are effective because of the presence of an electroactive imine group that facilitates easy adsorption on to the surface of a substrate metal. This effectiveness can be improved if the moiety possesses aromaticity/multiple bonds and participation of other hetero atoms/functional groups by facilitating electronic interaction with that of the d-orbital of Fe. Studies by various research groups suggest that the choice of Schiff bases as a corrosion inhibitor would be a successful strategy. The environment-friendly nature of the corresponding compounds is an added advantage to consider this for industrial applications.[5,15,17−19]

The Schiff bases synthesized from 4-amino-antipyrine (AAP) and suitable aldehydes have exhibited several functional properties such as antimicrobial, antioxidant, leishmanicidal, and corrosion inhibition due to their chemical structure and nature. There are very few detailed studies of AAP-based Schiff bases applied as a corrosion inhibition. Govindaraju et al. studied the synthesis and applications of AAP-based Schiff bases as corrosion inhibitors for MS in 1 M HCl.[1] Different aldehydes were used to synthesize the Schiff base and evaluated using conventional gravimetric analysis and electrochemical experiment. Junaedi et al. employed a Schiff base produced from the composition of AAP and 4-nitrobenzaldehyde on MS in a 1 M Hydrochloric acid solution.[2] The efficiency of the Schiff base obtained from AAP and substituted benzaldehydes was successfully evaluated by Eldesoky's group in a 2 M HNO_3 medium.[3] The same molecules also exhibited an appreciable performance in a 2 M HCl solution.[4] Balaji et al. proved the suitability of these Schiff

Received: December 15, 2023
Revised: February 23, 2024
Accepted: February 28, 2024
Published: March 8, 2024

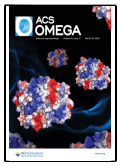

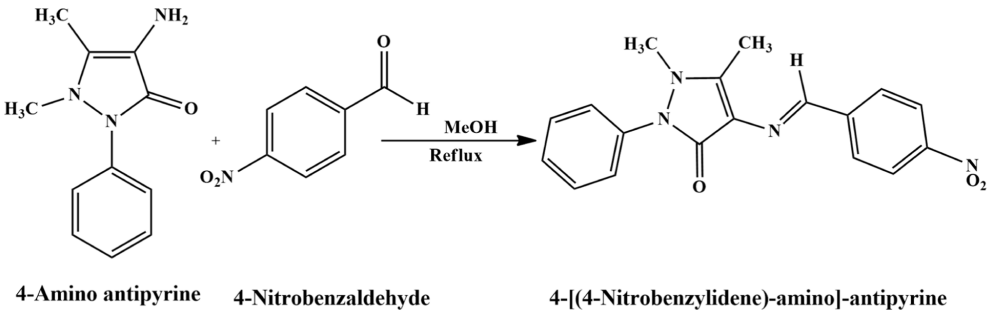

Figure 1. (Reaction scheme 1) molecular structure of 4-[(4-nitro benzylidene)-amino]-antipyrine (4-NBAAP).

bases prepared by composing AAP with different aldehydes such as 4-Nitrobenzaldehyde for MS in 1 M HCl.[5] Transition-metal complexes of AAP-based Schiff bases also have performed as corrosion inhibitors along with biological activities.[6] P110 steel, which is a medium carbon grade alloy steel, was studied in highly concentrated acid solution in the presence of AAP-based Schiff bases prepared with benzaldehyde and 4-nitrobenzaldehyde.[7] Substituted benzaldehydes were used to prepare Schiff bases with AAP and evaluated for their inhibition efficiency in an acidic medium by Upadhyay et al.[8] Abbass et al. studied the efficacy of 2-dimethylaminopropionamidoanti-pyrine in 1 M HCl to inhibit MS corrosion with the help of experimental and theoretical methods.[9] A series of Schiff bases derived from some amino benzoic acid and AAP were synthesized by Okey and team, and their inhibition efficiency was tested in an aggressive 1 M HCl medium.[10] Substituted benzaldehydes were composed of AAP, and the resulting compounds were evaluated for their inhibition mechanism by Madi et al.[11] Raheef et al. prepared an AAP-based Schiff base using 2-aminothiozole and studied it in 1 M HCl for its efficiency and found appreciable inhibition.[12] Hanoon and group conducted research on 4-((4-(dimethylamino)benzylidine)amino)antipyrine and found its appreciable inhibition capacity for MS material in 1 M HCl.[13] A research group led by Aziz synthesized an AAP-based Schiff base composed of 2-methylbenzaldehyde and studied its inhibition efficiency in 1 M HCl for MS.[14] Previous literature reports related to the Schiff base synthesized by composing AAP and 4-nitrobenzaldehyde were limited to either experimental studies or particular substrate material/corrosive medium.[4,8,11] Application of this inhibitor molecule in a very aggressive and common industrially employed corrosive medium along with detailed experimental and theoretical evaluation is lacking in the literature. In this direction, the current contribution aims to evaluate corrosion inhibition efficiencies of a Schiff base synthesized using AAP and 4-nitrobenzaldehyde for MS material in 1 M hydrochloric acid solution.

2. EXPERIMENTAL DETAILS

2.1. Chemicals and Materials. The heterocyclic compounds, 4-amino-antipyrine ($C_{11}H_{13}N_3O$) and 4-nitrobenzaldehyde ($C_7H_5NO_3$), were obtained from SRL Pvt. Ltd. Methanol (MeOH) was received from Merck. The above chemicals were used in Schiff base synthesis. FTIR analysis was performed utilizing the PerkinElmer Fourier transform infrared spectroscopy instrument. The Varian Mercury 400 MHz ^{1}H NMR spectra were obtained through mass spectrum analyses using an Agilent 6224 HRMS spectrometer, with TMS serving as the internal standard. A Varian Mercury (VM) 100 MHz spectrometer was used to examine the ^{13}C NMR data. ^{13}C NMR chemical shifts (δ) were reported in ppm using the internal $CDCl_3$ M 77.0 ppm.[15−17,20]

MS material was utilized to perform corrosion tests with the following compositions: 0.04 C, 0.022 P, 0.35 Mn, 0.036 S. MS specimens with dimensions of 0.1 × 3 × 3 cm were employed for gravimetric tests, whereas, for electrochemical experiments, a 1 cm^2 exposed area and a 5 cm long stem were isolated using Araldite resin in the samples. MS samples were rubbed with emery papers of grades 220, 660, and 1200 as part of the pretreatment process. The samples were cleaned with double-distilled water and acetone, dried, and kept in a desiccator.[16−18,24,25]

2.2. Experimental Methods. *2.2.1. Synthesis.* The Schiff bases were synthesized and characterized by using physicochemical methods. The synthetic route for the synthesis of the Schiff base is given in Scheme 1. The Schiff base, 4-[(4-nitro benzylidene)-amino]-antipyrine (4-AAPNB), was prepared (as shown in Reaction Scheme 1) by an equimolar mixture (1:1) of methanolic medium of 4-amino-antipyrine (0.2000 g) and 4-nitrobenzaldehyde (0.122 g) in a round-bottom flask. In addition, 30 mL of methanol (MeOH) was added followed by a 4 h reflux at 303 K. An orange/yellowish colored precipitate thus obtained was purified and filtered through two to three methanol washes to eliminate any remaining reactants and then vacuum-dried. Analytical grade chemicals and double-distilled water were used for the entire experiment. Molecules thus prepared were utilized for further studies (Figure 1).[15−19,57,58]

2.2.2. Characterization of 4-[(4-Nitrobenzylidene)-amino]-antipyrine. FTIR, 1H NMR, 13CNMR, and Mass Spectral Analysis.

Yield: 0.61 g (81%),

Melting point: 116−120 °C.

Solubility: soluble in polar solvents such as water, methanol, ethanol, ethyl acetate, acetonitrile, non-polar solvent toluene.

Anal. Calcd for $C_{17}H_{16}N_4O_3$ (336.12): C, 64.28; H, 4.79; N, 16.66; O, 14.27.

Elemental analysis (CHN): C, 64.28; (100.0%) H, 4.79; (19.8%) N, 16.66; (2.5%) O, 14.27.

FTIR: 3047.4 ν (aromatic C−H), 16,702.1 ν(C═O), 1526.3 ν(C═N).

^{1}H NMR of 4-[(4-nitro benzylidene)-amino]-antipyrine shows the presence of peaks 9.505 (s,1H), 8.423 (s,1H), 7.484−7.527 (m,4H), 7.601−7.621 (d,3H), 7.226 (s,1H), 6.869−6.889 (d,3H), 3.728 (s,3H). ^{13}C NMR 160.776, 158.498, 157.706, 145.545, 143.114, 140.882, 130.824, 129.498, 125.490, 122.648, 117.688, 114.144, 104.810, 99.012, 55.428.

Mass: 337.06 m/z (100%).[19−24] (Figure S1)

https://doi.org/10.1021/acsomega.3c10048
ACS Omega 2024, 9, 13262−13273

2.2.3. Medium. Analytical reagent grade 37% hydrochloric acid was diluted to prepare 1 M HCl using double-distilled water. Acidic solutions for corrosion study were prepared by dissolving a specific amount of corrosion inhibitor molecules in 1 M HCl.[24−27]

2.2.4. Inhibitor Solutions. The desired concentrations of inhibitor solutions (10, 30, and 50 μM) were prepared by dissolving a specified amount of 4-[(4-nitro benzylidene)-amino]-antipyrine (4-NBAAP) in 1 M HCl solutions.[23,24]

2.3. Gravimetric Analysis. Different MS strips were immersed in 1 M HCl media having different concentrations of the 4-NBAAP inhibitor for about 4 h at room temperature. The weight differences of MS strips without and with the inhibitor were recorded and used to calculate the inhibition efficiency (IE %).[25−28]

2.3.1. Electrochemical Analysis. The electrochemical experiments, including a three-electrode, were adopted using a CHI 608C electrochemical analyzer (CH Instruments, 3700 Tennison Hill Drive, Austin, TX 78738). The working electrode was the MS sample with a 1 cm^2 exposed area and Sat. Calomel and Pt were reference and auxiliary electrodes, respectively. Samples were allowed to get stabilized over a period of 30 min for their open circuit potential (OCP) before every electrochemical experiment.[25−29]

2.3.2. Potentiodynamic and Polarization Studies. The potentiodynamic polarization studies were performed over a potential from +200 to −200 mV at the OCP with a scan rate of 0.5 mV s^{-1}. Corrosion characteristics such as corrosion potential (E_{corr}), corrosion current (I_{corr}), and anodic (β_a)/cathodic (β_c) Tafel slopes were obtained from the installed software.

The following relation was used to calculate the inhibition efficiencies (IE %) based on the obtained I_{corr} values.[27,30]

$$\eta\ \% = \frac{I_{corr}^{0} - I_{corr}^{1}}{I_{corr}^{0}} \times 100 \quad (1)$$

where I_{corr}^{0} and I_{corr} are the corrosion current densities without and with 4-NBAAP, respectively.

2.3.3. Electrochemical Impedance Spectroscopy. The electrochemical impedance spectroscopy (EIS) measurements were carried out in the frequency range of 1−10 MHz at corresponding OCP with an excitation signal of 5 mV. The obtained impedance results were analyzed with ZSimp-Win 3.21 software.[33−35]

With the help of the following equation, the inhibition efficiency was evaluated.

$$\eta\ \% = \frac{R_{ct} - R_{ct}^{0}}{R_{ct}} \times 100 \quad (2)$$

where R_{ct} and I_{ct}^{0} are the charge transfer resistance with and without 4-NBAAP, respectively.

Potential values reported were with reference to the Sat. Calomel electrode. The reported values were the mean of triplicate measurements.[27−35]

2.4. Morphological Studies. A scanning electron microscope Tescan Vega 3 was used to study morphological changes with corrosion in the presence and absence of the tested inhibitor in a corrosive medium. The working distance was 15 mm with an electron voltage of 15 kV and a magnification of 1000×, and a secondary electron detector was used to capture the images.

2.5. Quantum Chemical Studies. Quantum chemical calculations were carried out by using Gaussian 09 software and its time-dependent extension TDDFT at the CAM-B3LYP/6-31G level to ascertain the correlation between the molecular and electronic structure and inhibition efficiency of 4-NBAAP.

3. RESULTS AND DISCUSSION

3.1. Structural Analysis. Results are provided in the Supporting Information.

3.1.1. UV−Vis Analysis. The bands in the region of 265−280 nm are assigned to the $\pi-\pi^*$ transitions of the aromatic rings. The band at 309−357 nm involves an $n-\pi^*$ transition of the C═O and C═N groups. The longer wavelength band at 390−402 nm can be assigned to an intramolecular charge transfer transition. The charge transfer will originate from a 4-aminoantipyrine ring as an origin to the C═N group as a sink.[20,21,29] (Figure S2)

3.1.2. FT-IR Spectral Studies. The FT-IR spectra of the ligands exhibit intense bands at 1635−1650 and 1610−1620 cm^{-1} corresponding to antipyrine exocyclic ketone ν(C═O) and azomethine ν(CH═N), respectively. The band in the region of 1285−1310 cm^{-1} is assigned to phenolic ν(C−O). Thus, a ligand is tridentate in nature with O, N, O coordination sites. In the spectrum, ν(CH═N), i.e., around 1600 cm^{-1} confirms the presence of azomethine nitrogen.[22,23,30,31,57] (Figure S3)

3.1.3. NMR Spectroscopy. The ^{1}H NMR spectra of the ligands (Figures S4 and S5) display two sharp signals (3H) at δ 2.4 and δ 3.10−3.19 ppm corresponding to the (═C−CH_3) and N−CH_3 groups, respectively. A singlet (1H) observed at 9.7−10.6 ppm in the spectra of ligands has been assigned to an azomethine proton (−CH═N). A sharp singlet (1H) appeared for the o−OH proton of the ligand in the region δ 12−14 ppm.[21,22] In the ^{13}C NMR spectra of the molecule, the azomethine carbon resonance is observed at the 154 ppm range. The resonances for C−N and C−O are observed in the regions 145 and 160 ppm, respectively. The ^{13}C NMR spectra of complexes revealed the presence of six different carbons (119, 129, 143, 143, 149, and 159 ppm). The three quaternary carbons arising from aromatic units are in the same magnetic environments.

3.2. Gravimetric Analysis. The 100 cm^3 of 1 M hydrochloric acid was taken in beakers for the purpose of measuring weight loss. After the first beaker was fixed as an uninhibited blank solution, the remaining five beakers were filled with 1, 10, 30, and 50 μM concentrations of the inhibitor. In each of the five inhibited solutions, polished and pretreated MS strips were immersed for approximately 4 h (298 K). We measured the weight variations of each strip both before and after they were immersed in the solution (Figure S6). The corrosion rate for each strip is provided by the following equation

$$\gamma_{corr} = \frac{\Delta m}{St} \quad (3)$$

where Δm is the corrosion weight loss of the MS (mg), S is the surface area of the MS sample (cm^2), and t is the time of exposure.

The percentage inhibition efficiency η_w (%) was calculated using the relationship

https://doi.org/10.1021/acsomega.3c10048
ACS Omega 2024, 9, 13262−13273

Table 1. Corrosion Parameters Obtained by the Weight Loss Measurement in 1 M Hydrochloric Acid at Room Temperature at 298 K

	concentration	W_0	W_1	$W_{(g)}$	θ	η %	CR (mgcm^{-2} h^{-1})
4 h	blank	1.576	1.466	0.11	0.0698		1.2×10^{-5}
	1 μM	1.6568	1.631	0.0258	0.01557	76.54	2.9×10^{-6}
	10 μM	1.6977	1.6722	0.0255	0.01502	76.81	2.8×10^{-6}
	30 μM	1.6279	1.6073	0.0206	0.01265	81.27	2.3×10^{-6}
	50 μM	1.7214	1.704	0.0174	0.01011	84.18	1.9×10^{-6}

Table 2. Corrosion Parameters at Different Temperatures[a]

C (mM)	temperature											
	298 K			313 K			323 K			333 K		
	CR (mg cm^{-2} h^{-1})	η_w (%)	Θ	CR (mg cm^{-2} h^{-1})	η_w (%)	θ	CR (mg cm^{-2} h^{-1})	η_w (%)	Θ	CR (mg cm^{-2} h^{-1})	η_w (%)	θ
blank	1.2×10^{-5}			1.5×10^{-5}			2.1×10^{-5}			5.7×10^{-5}		
1 μM	1.2×10^{-6}	89.81	0.89818	1.81×10^{-6}	87.74	0.87744	1.4×10^{-5}	34.15	0.34157	3.9×10^{-5}	30.80	0.3080
10 μM	6.4×10^{-7}	94.72	0.94727	1.51×10^{-6}	89.77	0.89774	1.2×10^{-5}	41.73	0.41736	3.5×10^{-5}	37.82	0.3782
30 μM	4×10^{-7}	96.72	0.96727	1.46×10^{-6}	90.15	0.9015	1×10^{-5}	52.10	0.52105	2.9×10^{-5}	48.43	0.4843
50 μM	2.8×10^{-7}	97.72	0.97727	6.33×10^{-7}	95.71	0.95714	6.8×10^{-6}	67.94	0.67947	2.1×10^{-5}	62.13	0.6213

[a]Figure S6.

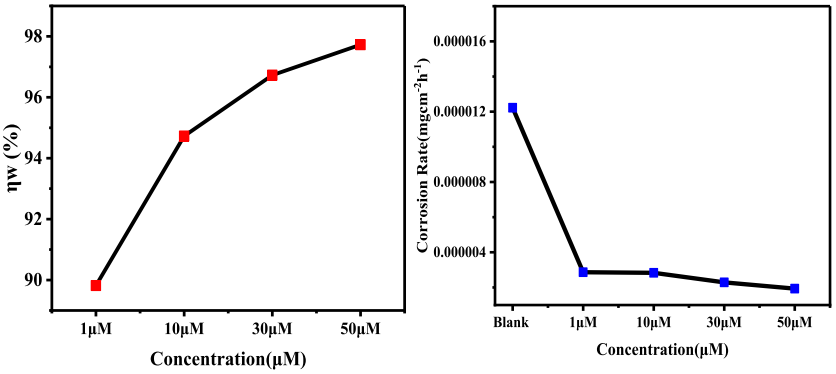

Figure 2. Corrosion efficiency and corrosion rate variation with different inhibitor concentrations.

$$\eta\ \% = \frac{\gamma^0_{corr} - \gamma^1_{corr}}{\gamma^0_{corr}} \times 100 \quad (4)$$

where γ^0_{corr} and γ^1_{corr} are the corrosion rates (CR) of the MS in the absence and presence of 4-[(4-nitrobenzylidene)-amino]-antipyrine, respectively (Table 1).

3.2.1. Effect of Temperature. We examined weight loss measurements in the 298−333 K temperature range both with and without 4-NBAAP in a 1 M HCl solution to ascertain how temperature affects the process of corrosion inhibition. Table 2 provides the basis for the corrosion parameters that are derived from weight loss measures. An increase in temperature rates upward of the evolution of hydrogen gas increases the rate at which MS oxidizes. As a result, as the temperature increases, the amount of inhibitor adsorption decreased and the MS dissolved more quickly.[26−35] In the current investigation, corrosion rates rise and inhibition efficiency falls in 1 M HCl media at constant concentrations of 4-NBAAP. Higher temperatures do not support the adsorption of inhibitor molecules, which is the reason behind this observation (Figures 2 and 3).

3.2.2. Adsorption Isotherm and Thermodynamic Consideration. Figure 4 depicts the adsorption isotherm concerning the way in which inhibitor molecules interact with the metal surface. Among different adsorption isotherm models that we fitted to the experimental data, the Langmuir isotherm was found to be the best fit. Figure 4, also shows few isotherm systems as an example, which are not fitting well with the experimental values, showing lower values for regression coefficients. Adsorption of 4-NBAAP on MS surfaces in

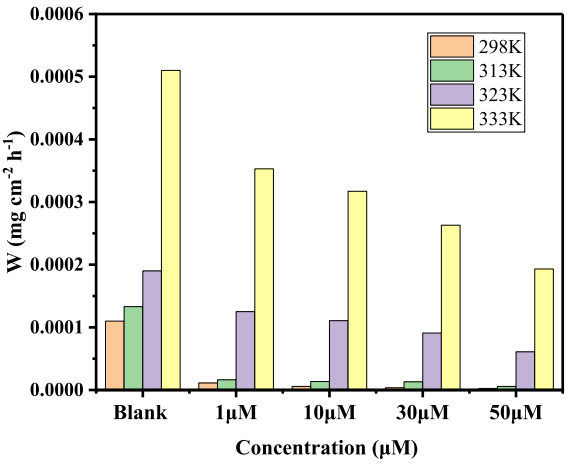

Figure 3. Effect of temperature on weight loss in 1 M HCl at different concentrations of the inhibitor (Figure S6).

https://doi.org/10.1021/acsomega.3c10048
ACS Omega 2024, 9, 13262−13273

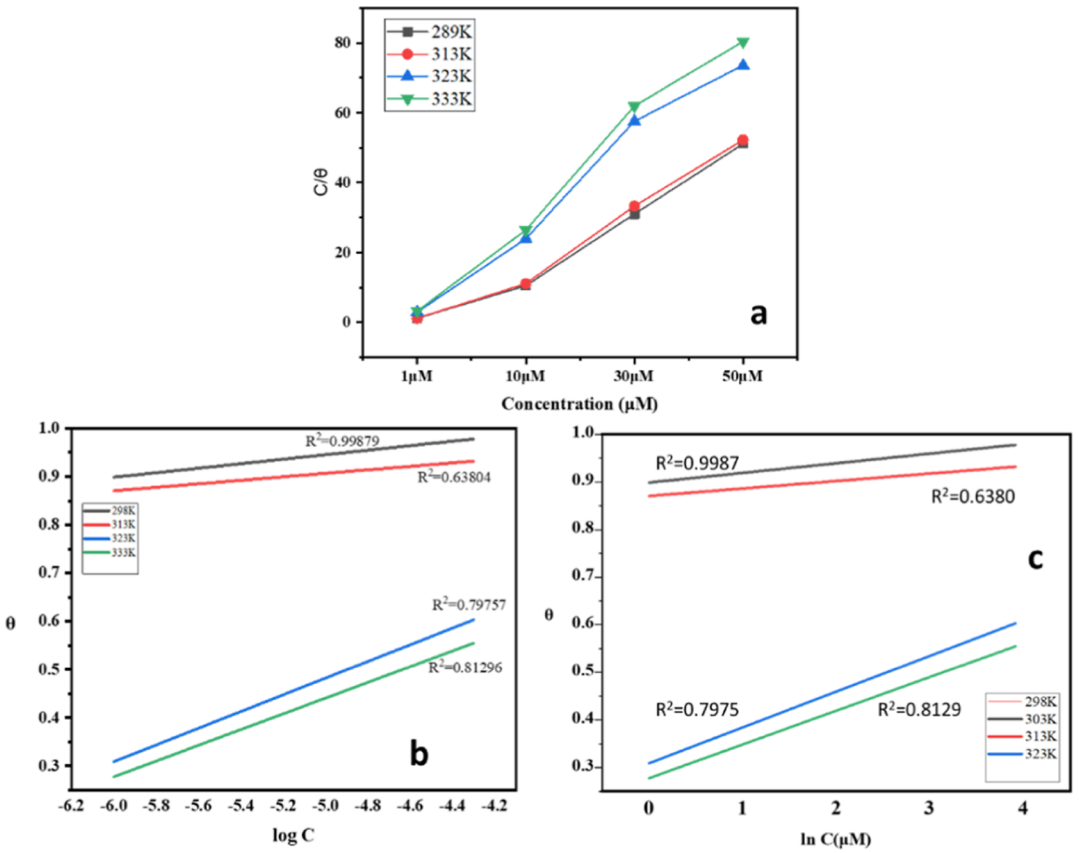

Figure 4. (a) Langmuir (b) Temkin, and (c) Freundlich adsorption isotherm plots of 4-NBAAP in a 1 M HCl solution on the MS surface.

hydrochloric acid follows the Langmuir adsorption isotherm, which can be mathematically expressed as follows.

$$\frac{C}{\theta} = \frac{1}{K_{ads}} + C \tag{5}$$

where C is the inhibitor concentration, θ is the degree of the surface coverage, and K_{ads} is the adsorption equilibrium constant.

The Langmuir adsorption isotherm plots and the corresponding C/θ vs C plots obtained for 4-NBAAP are linear with a nearly unit slope, which are presented in Figures 4 and 5. The standard free energy of adsorption (ΔG^0_{ads}) and the K_{ads} can be determined using the intercepts of the straight lines on the C/θ axis.[26]

$$K_{ads} = \frac{1}{55.5} \exp \frac{\Delta G^0_{ads}}{RT} \tag{6}$$

where R is the universal gas constant, T is the thermodynamic temperature, and 55.5 is the molar concentration of water in the media.

The adsorption parameters are shown in Table 3. The stability of the adsorbed layer on the MS surface in 1 M hydrochloric acid media and the spontaneity of the adsorption process can be related to the large negative values of ΔG^0_{ads}.[33] In general terms, physisorption is associated with ΔG^0_{ads} values of −20 kJ mol^{-1} or less, and chemisorption is indicated by values of −40 kJ mol^{-1} or more.[34] However, in 1 M HCl solutions, the calculated ΔG^0_{ads} values are between −40 and −20 kJ mol^{-1}. Both chemisorption and physisorption are involved in the adsorption of 4-NBAAP on a MS.

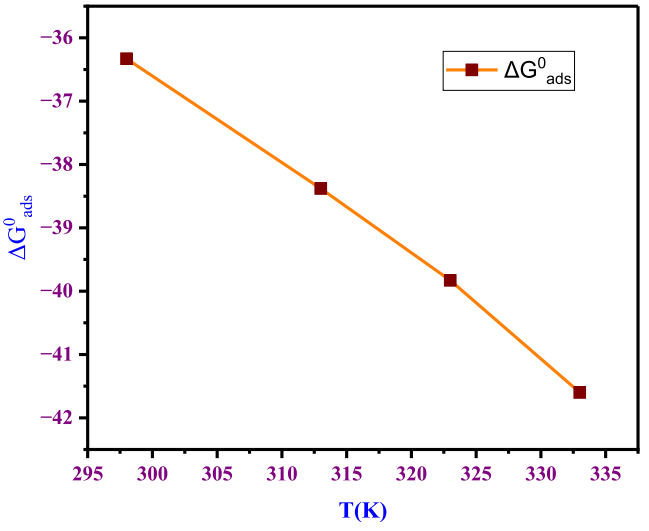

Figure 5. Relation between temperature (T) and ΔG^0_{ads} (kJ mol^{-1}).

In general, as the temperature increases, ΔG^0_{ads} increases (become less negative), signifying an exothermic process; and decrease in ΔG^0_{ads} (becomes more negative) indicates the process to be an endothermic one. Table 3 makes it evident that as temperature rises, ΔG^0_{ads} rises as well, indicating that 4-NBAAP corrosion inhibition of MS is an exothermic process. Here, adsorption of 4-NBAAP on the metal surface becomes unfavorable as the reaction temperature rises.[35−45] The integrated version of the Van't Hoff equation can be used to calculate the entropy of adsorption and the enthalpy of adsorption (ΔH^0_{ads}) and it is expressed as follows.[46−54]

https://doi.org/10.1021/acsomega.3c10048
ACS Omega 2024, 9, 13262−13273

Table 3. Thermodynamic Parameters of the Adsorption of 4-NBAAP on the MS Surface at Different Temperatures

temperature (K)	R^2	K_{ads} (M^{-1})	ΔG^0_{ads} (kJ mol^{-1})	ΔH^0_{ads} (kJ mol^{-1})	ΔS^0_{ads} (J mol^{-1} K^{-1})
298	0.9866	42,070	−36.33		−122.1
313	0.9831	45,690	−38.38	−72.56	−122.4
323	0.9614	49,700	−39.83		−123.1
333	0.9797	51,500	−41.6		−123.4

$$\Delta G^0_{ads} = \Delta H^0_{ads} - T\Delta S^0_{ads} \quad (7)$$

Figure 5 shows a linear plot of ΔG^0_{ads} against T, where the intercept is equal to ΔH^0_{ads} and the slope is equal to ΔS^0_{ads}. The values of ΔS^0_{ads} and ΔH^0_{ads} that were obtained are −123.4 and −72.56 kJ mol^{-1}, respectively.

The inhibitor adsorption on MS exhibits an exothermic behavior, as indicated by the negative values of ΔH^0_{ads}. An exothermic adsorption process typically denotes chemisorption or physisorption.[55] When examining the absolute value of ΔH^0_{ads}, one can differentiate between physisorption and chemisorption in an exothermic process. In the case where ΔH^0_{ads} is lower than that of 40 kJ mol^{-1}, it is considered to be physisorption, while that for chemisorption approaches the value approaching 100 kJ mol^{-1}.[44] In the present case, ΔH^0_{ads} is −72.56 kJ mol^{-1}; the existence of both physical and chemical adsorption is clearly observed in this intermediate case, and thus ΔG^0_{ads} and ΔH^0_{ads} values complement each other. As expected, the negative values of ΔS^0_{ads} pronounce the decrease in entropy with respect to an exothermic adsorption process. In a bulk solution, the inhibitor molecules are free to migrate and as the adsorption process proceeds, the inhibitor molecules' adsorption onto the MS surface becomes more organized, which lowers entropy.[46−56] Moreover, the values of two methods' results for ΔH^0_{ads} and $-\Delta S^0_{ads}$ are in good agreement.

3.3. Electrochemical Studies. *3.3.1. OCP Measurements.* OCP measurements were performed prior to the other electrochemical experiments. OCP signifies the equilibrium potential in the open circuit with no electrical interruption or without applying any external load. This equilibrium forms between the electrode surface and electrolyte interface, and it deviates in case of any change in the interface or reactions on the surface of the electrode.[21] Figure 6 presents OCP profiles for the steel specimens under different environments measured for 1800 s. The sample in 1 M HCl with no inhibitor attains −0.55 V, and the samples with different inhibitor concentrations attain potentials with least negative values, i.e., −0.542 V in the case of 50 μM. This proves that a higher concentration of the inhibitor facilitates the electrochemical stability of the steel specimen.

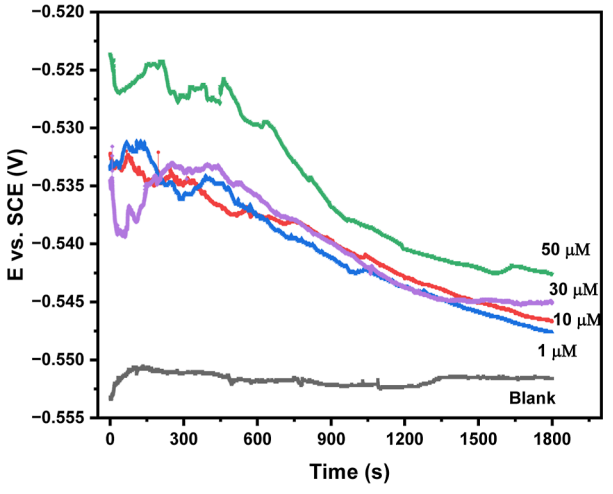

Figure 6. OCP profiles of the samples at 298 K with and without 4-NBAAP in 1 M HCl.

3.3.1.1. Potentiodynamic Polarization Studies. The potentiodynamic polarization curves of the samples in 1 M hydrochloric acid in the presence and absence of 4-NBAAP are shown in Figure 7. Table 4 shows the corrosion kinetic

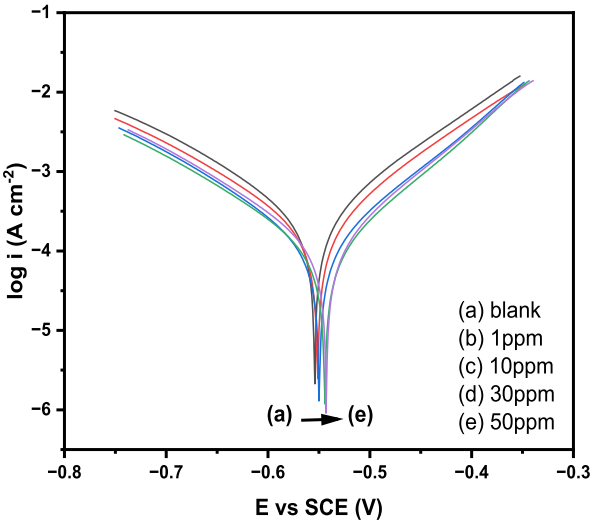

Figure 7. Plots of Tafel polarization for the samples at 298 K with and without 4-NBAAP in 1 M HCl.

Table 4. Potentiodynamic Polarization Parameters with and without Varying the 4-NBAAP Concentrations in 1 M HCl

C (μM)	$-E_{corr}$ (mV)	$-b_c$ (V^{-1})	$-b_a$ (V^{-1})	I_{corr} (μA cm^{-2})	standard deviation	η_T (%)
blank	483.7	9.282	11.271	270 ± 0.9	0.9	
1 μM	549.0	8.032	9.358	131 ± 1.2	1.2	51.48
10 μM	550.2	8.427	10.144	115 ± 2.3	2.3	57.40
30 μM	541.2	8.531	10.735	105 ± 2.1	2.1	61.11
50 μM	545.0	8.149	10.504	94 ± 1.5	1.5	65.18

parameters derived from these curves. Both the anodic and cathodic branches of the polarization curves of the acid solutions shifted toward a lower current density at all investigated concentrations in acid media, as the figure illustrates. This suggests that 4-NBAAP in the 1 M HCl solution inhibited both the anodic and cathodic reactions of MS corrosion. As inhibitor concentration rises, protection efficiency rises and corrosion current density falls. The addition of the inhibitor resulted in a positive shift in the E_{corr} values, and the values of β_c and β_a did not significantly change. Also, if and only if the E_{corr} shift is more than 85 mV, the inhibitor can be designated as either cathodic or anodic in nature. This

https://doi.org/10.1021/acsomega.3c10048
ACS Omega 2024, 9, 13262−13273

implies that 4-NBAAP functions as an inhibitor of a mixed type.[46,47]

The inhibition efficiency (eq 8) is enhanced as a result of the inhibitor molecule's increasing surface coverage (caused by an increase in inhibitor concentration). A maximum of 65% inhibition efficiency is seen at 298 K, which is corresponding to the inhibitor concentration of 50 μM.

$$\eta\ \% = \frac{I_{corr}^{0} - I_{corr}^{1}}{I_{corr}^{0}} \times 100 \tag{8}$$

3.3.2. Electrochemical Impedance Spectroscopy. Electrochemical impedance spectroscopy was used to assess MS corrosion behavior in 1 M hydrochloric acid with and without 4-NBAAP. The typical impedance data as Nyquist plots are shown in Figure 8 and Bode plots in Figure 9, and the corresponding parameters are presented in Table 5 with the equivalent circuit considered shown in Figure 10

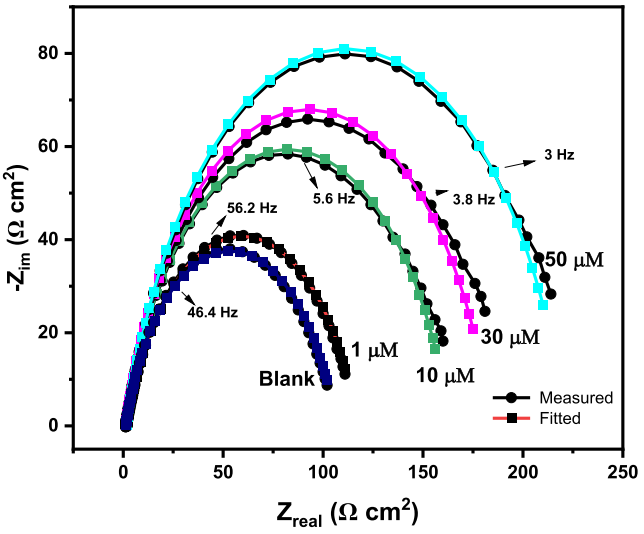

Figure 8. Nyquist plots of MS in 1.0 M hydrochloric acid without and with different concentrations of 4-NBAAP.

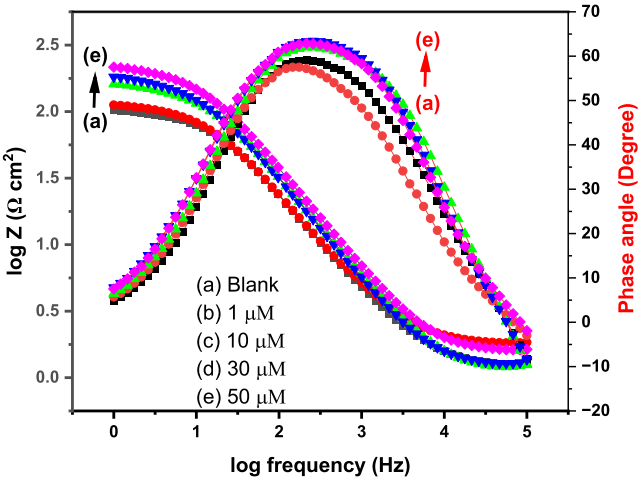

Figure 9. MS Bode plots in a 1 M HCl solution with and without varying the concentration of 4-NBAAP.

These graphs show that the addition of 4-NBAAP to 1 M hydrochloric acid dramatically altered the impedance response of the MS. Additionally, the impedance spectra are composed of a single capacitive loop, and as the inhibitor concentration rises, so does the diameter of the loops. This suggests that 4-NBAAP functions as the main interface inhibitor in hydrochloric acid media and that inhibitor adsorption happens via simple surface coverage.[46] The similar nature of Nyquist loops indicates that the mechanism of corrosion involved in the presence and absence of the inhibitor remains the same. For a more precise fit, a constant phase element (CPE) is used in place of the capacitive element (C_{dl}). The electrochemical equivalent circuit used to analyze the impedance data is shown in Figure 10. The fitting standard of the equivalent circuit was checked by the chi-square (χ^2) values. Generally, the values of χ^2 among 10^{-3} and 10^{-5} suggest an ideal fit.[48] The proposed equivalent circuit provided fairly small ($<5 \times 10^{-3}$) χ^2 values, suggesting a satisfactory fitting of the obtained impedance spectra to the proposed equivalent circuit.

$$\eta_z\% = \left(\frac{R_{ct} - R_{ct}^{0}}{R_{ct}}\right) \times 100$$

The CPE impedance (Z) can be expressed as

$$Z_{CPE} = Q^{-1}(j\omega)^{-n} \tag{9}$$

where Q is the CPE, ω is the angular frequency, j^2 is -1, n is the CPE exponent, and C_{dl} is the double-layer capacitance.[49]

Using the following formula, C_{dl} values can be obtained

$$C_{dl} = (QR_{ct}^{1-n})^{1/n} \tag{10}$$

As the inhibitor concentration in hydrochloric acids increases, it is clear from the table that Q falls and R_{ct} increases. A protective layer forming on the electrode surface is the reason for the increase in R_{ct}.[44] By contrast, a decrease in the local dielectric constant and/or an increase in the electrical double layer's thickness could have caused the C_{dl} to drop.[45−56] With a higher concentration of hydrochloric acids, 4-NBAAP's protection efficacy rises. As observed in the Bode plots, the increase in mod Z and phase angle shift with increased inhibitor concentration are attributed to the better inhibition performance. Here, increased inhibitor concentration results in progress in film formation and surface coverage, which is reflected in the shift and increase in the phase angle values. "n" indicates the surface roughness or surface inhomogeneity, and a slight variation in its value can be ascribed to minimization of surface inhomogeneity due to the adsorption of inhibitor molecules on the active adsorption sites.[44−56] According to these findings, 4-NBAAP inhibits MS corrosion effectively in aggressive HCl solution, and it works wonderfully as an MS corrosion inhibitor. Potentiodynamic polarization curves and EIS-obtained inhibition efficiencies agree fairly well.

While our results were compared with the literature reports, the following observations were made. Govindaraju et al. studied the synthesis and applications of AAP-based Schiff bases obtained from different aldehydes and AAP, and the maximum inhibition efficiency obtained was 90.83% at 0.008 M.[1] 4-Nitrobenzaldehyde and AAP Schiff base studied by Junaedi et al.[2] shows an efficiency of 87% at 0.5 mM in 1 M HCl solution. Eldesoky's group, which produced Schiff bases from substituted benzaldehydes, showed their maximum efficiency in the range of 41−48% in 2 M HCl.[4] 2-Dimethylaminopropionamidoanti-pyrine exhibited a highest inhibition of 91.9% at a 5 mM concentration of the inhibitor in 1 M HCl.[9] Experimental results obtained for the Schiff base

https://doi.org/10.1021/acsomega.3c10048
ACS Omega 2024, 9, 13262−13273

Table 5. Electrochemical Impedance Parameters of MS in 1 M Hydrochloric Acid Containing Different Inhibitor Concentrations

C (μM)	R_S (Ω^{-1} cm^{-2})	R_{ct} (Ω cm^{-2})	standard deviation	Q ($\mu\Omega^{-1}$ Sn cm^{-2})	n	C_{dl} (μF cm^{-2})	$\chi^2 \times 10^{-3}$	η_Z (%)
blank	1.25	104.9 ± 1.2	0.96	250	0.79	4.7461	3.05	
1	1.79	115.3 ± 1.6	1.6	240	0.78	4.2924	1.04	31.19
10	1.17	162.3 ± 1.3	1.69	160	0.80	3.5565	4.96	35.36
30	1.23	182.9 ± 0.9	0.9	160	0.81	3.2884	3.83	42.64
50	1.55	220.3 ± 0.8	0.8	140	0.81	3.1870	1.08	52.65

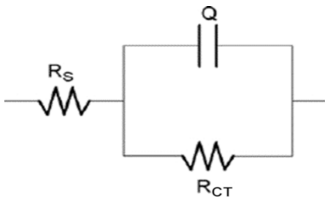

Figure 10. Electrochemical equivalent circuit model used to fit the impedance data. R_s = solution resistance, R_{ct} = charge transfer resistance, and Q = CPE.

obtained from amino benzoic acid and AAP show the corrosion inhibition to be up to 97% at a 1 mM inhibitor concentration.[10] The efficiency of Schiff bases designed from substituted benzaldehydes and AAP claimed to be efficient up to 95.03% at a 0.0005 M inhibition concentration according to the experiments performed.[11] The compound prepared out of 2-aminothiozole and AAP showed 88% efficacy at a 500 ppm concentration.[12] 95% efficiency toward corrosion inhibition was reported in the case of 4-((4-(dimethylamino)-benzylidine)amino)antipyrine at 0.5 mM[13] *N*-2-methylbenzylidine-4-antipyrineamine, 91.8% at 5 × 10^{-4} M.[14]

3.4. Surface Morphological Study. To establish the corrosion inhibition of 4-NBAAP, morphological studies were carried out and SEM images of the metal surfaces were analyzed. Figure 11a–c represents the surface morphology of the metal surfaces in different conditions such as in the bare

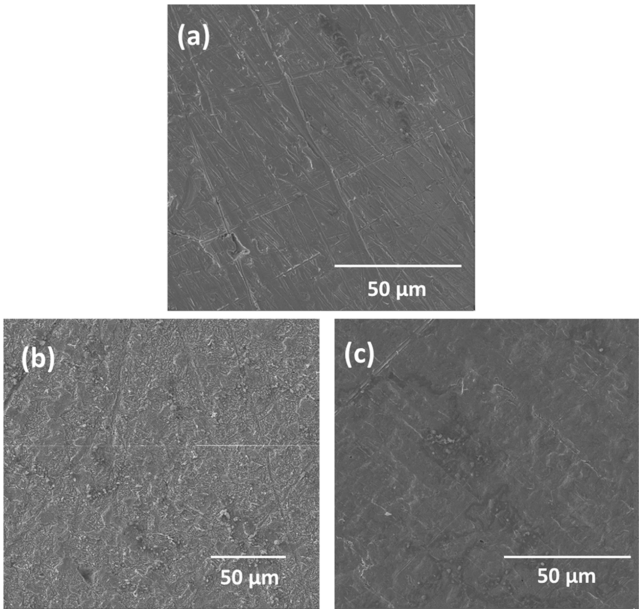

Figure 11. SEM images of the metal samples at different conditions: (a) bare and (b) after immersion for 4 h in 1 M HCl without the inhibitor and (c) with the inhibitor.

condition and after 4 h of immersion in an uninhibited solution and an inhibited solution, respectively. In the absence of the inhibitor, the steel sample degraded significantly, and rust formation was visible. However, in the presence of the inhibitor, the rate of rust formation was diminished, lessening the metal degradation and proving the inhibition capacity of 4-NBAAP in an aggressive corrosive environment.

3.5. Quantum Chemical Calculations. The Gaussian software was used to optimize the structure of the inhibitor (Berny optimization using GEDIIS/GDIIS optimizer), and the optimized structures of both nonprotonated and protonated species along with active centers are presented in Figures 12 and 13. correspondingly. The distributions of the highest occupied molecular orbitals (HOMO) and lowest unoccupied molecular orbitals (LUMO) are shown in Figures 14 and 15, respectively. The Mulliken population is a good tool to probe adsorption centers present in an inhibitor molecule; these are negatively charged atoms in the molecule, and the same are highlighted in Figures 12 and 13. The general consensus is that adsorption centers are the negatively charged heteroatoms and negatively charged carbon atoms of an aromatic ring. The more the magnitude and the number of negative charges present in a molecule, the more it is adsorbed on to the metal surface. The total negative charge (TNC) value would be an important parameter to quantify the adsorption centers present in a molecule. A higher TNC value indicates a larger charge separation and hence the presence of good adsorption sites. The TNC for the neutral and protonated inhibitor molecule from the DFT calculations was found to be −5.069 and −5.429, respectively, which is in support of the protonated counterpart. Figures 14 and 15 indicate that the HOMO and LUMO are predominantly distributed over the $-NO_2$ substituted benzene ring, pyrazolone ring, imine group, and hetero atoms, making them active centers in the inhibitor molecule for the adsorption on the steel surface.[20]

The obtained quantum chemical parameters of neutral and protonated species of the inhibitor are not similar, and they differ significantly because of the difference in electron density distribution between neutral and protonated inhibitor molecule. Besides, the values of E_{HOMO} and E_{LUMO} in the case of the protonated molecule imply its interaction with the metal surface via electron donation to the unoccupied d orbital of the metal and/or by accepting electrons easily from the same. Generally, a high value of dipole moment (μ) and small value of energy gap (ΔE) favor the strong interaction of the inhibitor molecule on the metal surface, which is true in the case of the protonated counterpart of 4-NBAAP. In addition, a higher dipole moment w.r.t. the protonated inhibitor is ascribed to dominant dipole–dipole interactions (Table 6).[21]

3.6. Mechanism of Inhibition. From potentiodynamic polarization results, it is affirmed that the molecule behaves as a mixed type of inhibitor. Corrosion inhibition is very much dependent on the extent to which the inhibitor adsorbs on the

https://doi.org/10.1021/acsomega.3c10048
ACS Omega 2024, 9, 13262–13273

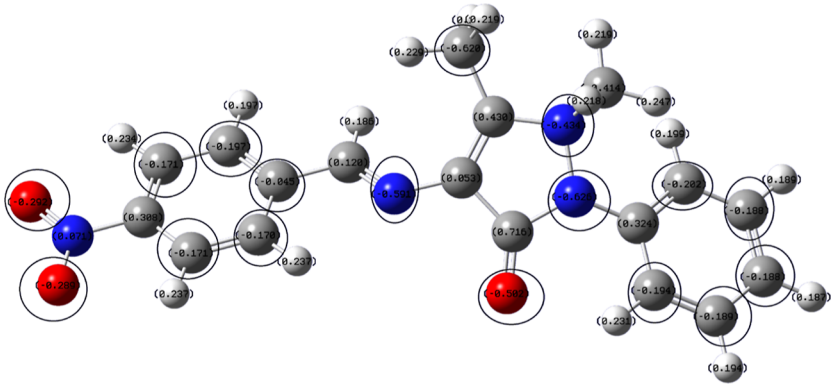

Figure 12. Optimized structure with a Mulliken charge distribution (negative charges encircled) of the 4-NBAAP molecule.

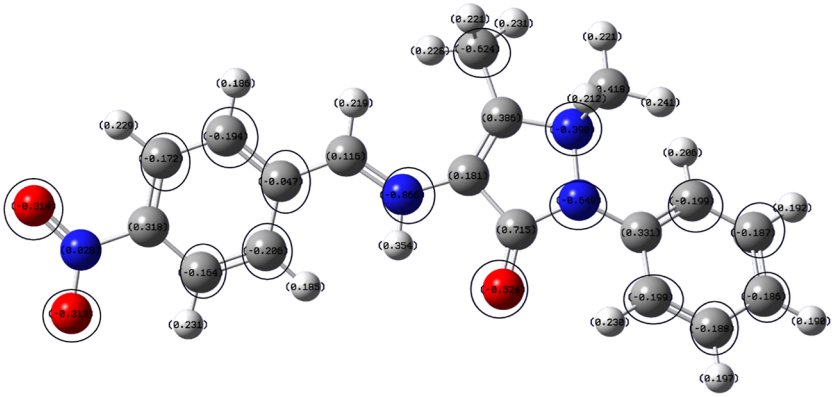

Figure 13. Optimized structure with a Mulliken charge distribution (negative charges encircled) of the protonated species of the 4-NBAAP molecule.

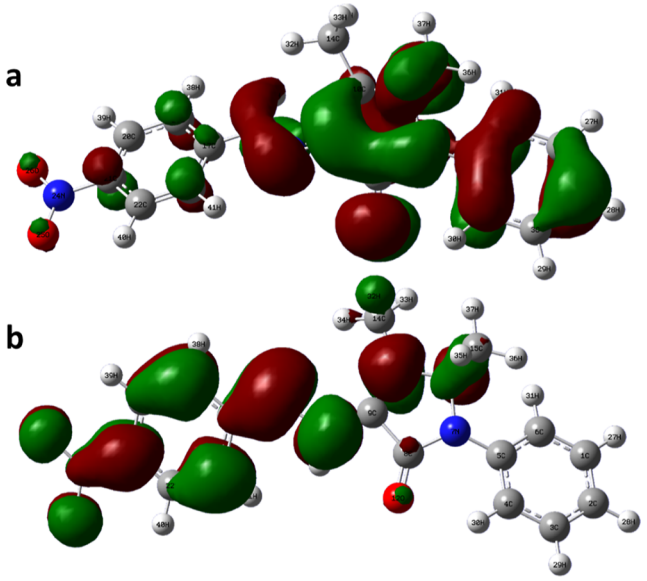

Figure 14. Frontier orbitals (HOMO) of (a) neutral and (b) protonated species of the 4-NBAAP molecule.

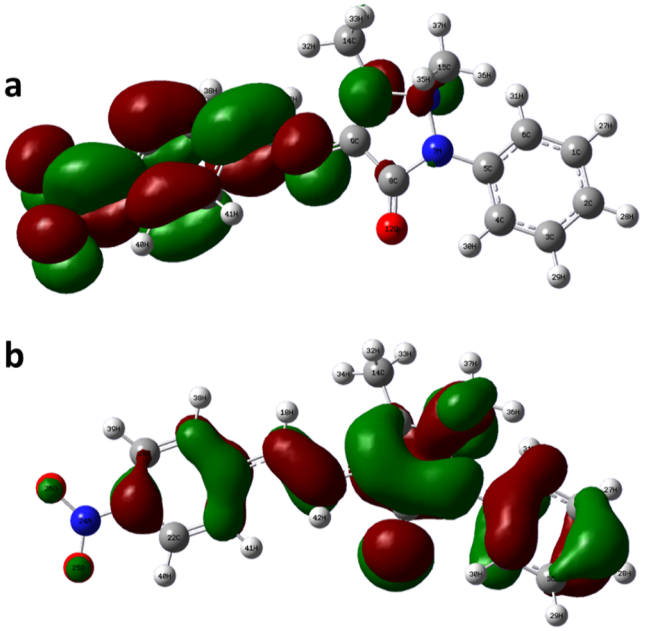

Figure 15. LUMO of the (a) neutral and (b) protonated species of the 4-NBAAP molecule.

metal surface, and this adsorption depends on the structure of the inhibitor, the nature and charge of the metal, and the type of corrosive medium. The corrosive medium (inhibitor completely dissolved in aqueous 1 M HCl solution, in the current study), in turn the solvent, plays a crucial role in achieving higher effectiveness of the inhibitor chosen. It has been claimed that the solvents function by decreasing the viscosity and ensuring the inhibitor formulation's stability in different environments. In addition, the solvent also is intended to improve the solubility, dispersibility, especially in acids, and wettability on the acid−steel interface.[59,60]

https://doi.org/10.1021/acsomega.3c10048
ACS Omega 2024, 9, 13262−13273

Table 6. Quantum Chemical Parameters of 4-NBAAP

quantum chemical parameters	neutral species of 4-NBAAP molecule	protonated species of 4-NBAAP molecule
E_{HOMO} (eV)	−5.78	−4.43
E_{LUMO} (eV)	−2.83	−6.15
ΔE (eV)	2.95	−1.72
dipole moment μ (Debye)	9.09	11.65
total energy (kcal/mol)	−711,464	−711,839

As 4-NBAAP possesses various active centers such as the imine group, $-NO_2$ substituted benzene ring, pyrazolone ring, etc., the adsorption phenomenon becomes complex to understand, and the following mechanism has been proposed. In an acidic medium, 4-NBAAP might be protonated at the N atom of the imine group, becoming a cation that exists in equilibrium with the corresponding neutral counterpart. The same can be represented as follows

$$4\text{-NBAAP} + nH^+ \leftrightarrow [(4\text{-NBAAP})H_n]^{n+}$$

Therefore, it is considered that in an acidic solution, the inhibitor exists as the protonated species and as a neutral molecule. The cationic form of the inhibitor 4-NBAAP is likely to adsorb directly at the cathodic sites, minimizing the hydrogen evolution reaction. At the corrosion potential, MS attains a positive charge when exposed to an acidic medium. This causes chloride ions from the medium to adsorb on the metal surface, leading to aggregation of negative charges toward the solution, favoring the adsorption of the protonated inhibitor onto the steel surface driven by electrostatic attraction (physisorption), controlling the anodic reaction, i.e., metal dissolution.[20,21] On the other hand, neutral 4-NBAAP may also adsorb at a positively charged steel surface via chemisorption by sharing electrons of electronegative atoms such as N and O and also by donor−acceptor interactions between π-electrons of antipyrine and benzaldehyde rings and the vacant d orbital of iron.[20,21] On the other hand, the protonated inhibitor molecule may also expected to be adsorbed directly on the cathodic sites in completion with hydrogen ions, thereby minimizing hydrogen evolution, the cathodic reaction. So, these interactions between the steel surface and the inhibitor molecule result in good adsorption, inhibiting the corrosion to a higher extent, which proves 4-NBAAP to be an excellent corrosion inhibitor in an aggressive HCl medium.

4. CONCLUSIONS

Results show that 4-NBAAP effectively inhibits MS corrosion in 1 M hydrochloric acid. By inhibiting both anodic and cathodic reactions, it functions as a mixed-type inhibitor. The rate of corrosion increases with temperature and decreases with the inhibitor concentration. The spontaneous and exothermic nature of 4-NBAAP adsorption is modeled by the Langmuir adsorption isotherm. Thermodynamic and kinetic parameters of the adsorption and corrosion processes are established. The trends obtained from the measurements of weight loss experiments are comparable to those of the electrochemical results. The variation in the surface morphology of metal samples in the presence and absence of the inhibitor molecule also pronounces the excellent protection ability of 4-NBAAP. Quantum chemical studies pronounced all our experimental conclusions to be in line and assisted in understanding the mechanism of corrosion inhibition.

■ ASSOCIATED CONTENT

Supporting Information

The Supporting Information is available free of charge at https://pubs.acs.org/doi/10.1021/acsomega.3c10048.

Mass, UV, FTIR, ^{1}H NMR, ^{13}C NMR spectral data; corrosion parameters in different inhibitor concentrations at different temperatures; weight loss experimentation; and images of synthesized crystals of the inhibitor (PDF)

■ AUTHOR INFORMATION

Corresponding Authors

Ranganatha Sudhakar − *Department of Chemistry, Presidency University, Bengaluru 560064, India;* orcid.org/0000-0001-8521-6887; Email: shashankaic@gmail.com

Shashanka Rajendrachari − *Department of Metallurgical and Materials Engineering, Bartin University, Bartin 74100, Turkey;* orcid.org/0000-0002-6705-763X; Email: kamath.ranganath@gmail.com

Authors

Ashwini Narayanswamy − *Department of Chemistry, Presidency University, Bengaluru 560064, India*

Dileep Ramakrishna − *Department of Chemistry, Presidency University, Bengaluru 560064, India*

P. V. Raja Shekar − *Department of Physics, SR University, Warangal 506371, India*

Complete contact information is available at: https://pubs.acs.org/10.1021/acsomega.3c10048

Notes

The authors declare no competing financial interest.

■ ACKNOWLEDGMENTS

The authors thank the Presidency University, Karnataka, India, for providing lab facilities.

■ REFERENCES

(1) Govindaraju, K. M.; Gopi, D.; Kavitha, L. Inhibiting Effects of 4-Amino-Antipyrine Based Schiff Base Derivatives on the Corrosion of Mild Steel in Hydrochloric Acid. *J. Appl. Electrochem.* **2009**, *39* (12), 2345−2352.

(2) Junaedi, S.; Al-Amiery, A.; Kadihum, A.; Kadhum, A.; Mohamad, A. Inhibition Effects of a Synthesized Novel 4-Aminoantipyrine Derivative on the Corrosion of Mild Steel in Hydrochloric Acid Solution Together with Quantum Chemical Studies. *Int. J. Mol. Sci.* **2013**, *14* (6), 11915−11928.

(3) Eldesoky, A. M.; Diab, M. A.; El-Bindary, A. A.; El-Sonbati, A. Z.; Seyam, H. A. Some Antipyrine Derivatives as Corrosion Inhibitors for Copper in Acidic Medium: Experimental and Quantum Chemical Molecular Dynamics Approach. *J. Mater. Environ. Sci.* **2015**, *6* (8), 2148.

(4) Eldesoky, A. M.; Ghoneim, M. M.; Diab, M. A.; El-Bindary, A. A.; El-Sonbati, A. Z.; Abd El-Kader, M. K. 4-Aminoantipyrine Schiff base derivatives as novel corrosion inhibitors for Q235 steel in hydrochloric acid medium. *J. Mater. Environ. Sci.* **2015**, *6* (10), 3066−3085.

(5) Balaji, M.; Chandrasekar, N.; Sharmila, G.; Manivannan, R. Synthesis and evaluation of anti-corrosive behavior of some schiff base derivative. *Int. J. Pure Appl. Res. Eng. Technol.* **2016**, *4* (6), 51−64.

(6) Kashyap, S.; Kumar, S.; Ramasamy, K.; Lim, S. M.; Shah, S. A. A.; Om, H.; Narasimhan, B. Synthesis, biological evaluation and corrosion inhibition studies of transition metal complexes of Schiff base. *Chem. Cent. J.* **2018**, *12* (1), 117.
(7) Singh, A.; Ansari, K. R.; Quraishi, M. A.; Savas, K.; Lei; Guo, d. Aminoantipyrine derivatives as a novel eco-friendly corrosion inhibitor for P110 steel in simulating acidizing environment: Experimental and computational studies. *J. Nat. Gas Sci. Eng.* **2020**, *83*, 103547.
(8) Upadhyay, A.; Purohit, A. K.; Mahakur, G.; Dash, S.; Kar, P. K. Verification of corrosion inhibition of Mild steel by some 4-Aminoantipyrine-based Schiff bases - Impact of adsorbate substituent and cross-conjugation. *J. Mol. Liq.* **2021**, *333* (333), 115960.
(9) Abbass, M. K.; Raheef, K. M.; Aziz, I. A.; Hanoon, M. M.; Mustafa, A. M.; Al-Azzawi, W. K.; Al-Amiery, A. A.; Kadhum, A. A. H. Evaluation of 2-Dimethylaminopropionamidoantipyrine as a corrosion inhibitor for mild steel in HCl solution: A combined experimental and theoretical study. *Prog. Color, Color. Coat.* **2024**, *17* (1), 1−10.
(10) Okey, N. C.; Obasi, N. L.; Ejikeme, P. M.; Ndinteh, D. T.; Ramasami, P.; Sherif, E. S. M.; Akpan, E. D.; Ebenso, E. E. Evaluation of some amino benzoic acid and 4-aminoantipyrine derived Schiff bases as corrosion inhibitors for mild steel in acidic medium: Synthesis, experimental and computational studies. *J. Mol. Liq.* **2020**, *315*, 113773.
(11) Mahdi, B. S.; Aljibori, H. S. S.; Abbass, M. K.; Al-Azzawi; Kadhum, A. H.; Hanoon, M. M.; Isahak, W. N. R. W.; Al-Amiery, A. A.; Sh Majdi, H. Gravimetric analysis and quantum chemical assessment of 4-aminoantipyrine derivatives as corrosion inhibitors. *Int. J. Corros. Scale Inhib.* **2022**, *11* (3), 1191−1213.
(12) Raheef, K. M.; Qasim, H. S.; Radhi, A. A.; Kh Al-Azzawi, W.; Hanoon, M. M.; Al-Amiery, A. A. Gravimetric and density functional theory investigations on 4-amioantipyrin schiff base as an inhibitor for mild steel in HCl solution. *Prog. Color, Color. Coat.* **2023**, *16*, 255−269.
(13) Hanoon, M.; Zinad, D. S.; Resen, A. M.; Al-Amiery, A. A. Gravimetrical and surface morphology studies of corrosion inhibition effects of a 4-aminoantipyrine derivative on mild steel in a corrosive solution. *Int. J. Corros. Scale Inhib.* **2020**, *9* (3), 953−966.
(14) Aziz, I. A. A.; Abdulkareem, M. H.; Annon, I. A.; Hanoon, M. M.; Al-Kaabi, M. H. H.; Shaker, L. M.; Alamiery, A. A.; Isahak, W. N. R. W.; Takriff, M. S.; Ahmed, A.; Alamiery, W.; Nor, R.; Wan, I.; Mohd, S. Weight loss, thermodynamics, SEM, and electrochemical studies on N-2-methylbenzylidene-4-antipyrineamine as an inhibitor for mild steel corrosion in hydrochloric acid. *Lubricants* **2022**, *10* (2), 23.
(15) Rahul, D. Schiff bases: synthesis, applications and characterization using FT-NMR spectroscopy. *J. Emerg. Technol. Innovat. Res.* **2018**, *5* (1), 1435.
(16) Dave, P. N.; Chopda, L. V. Schiff based corrosion inhibitors for metals in acidic environment: A review. *Mater. Sci. Eng.* **2018**, *2* (6), 258−267.
(17) Kumar, S.; Yogesh, C.; Swami, V. K. A Study of Newly Schiff Base as Corrosion Inhibitor for Metal Corrosion in Acidic Medium. *Int. J. Trend Sci. Res. Dev.* **2021**, *5* (5), 1945−1950.
(18) Vikneshvaran, S.; Velmathi, S. Schiff Bases of 2,5-Thiophenedicarboxaldehyde as Corrosion Inhibitor for Stainless Steel under Acidic Medium: Experimental, Quantum Chemical and Surface Studies. *ChemistrySelect* **2019**, *4* (1), 387−392.
(19) Shakeel Nawaz, S.; Manjunatha, K. B.; Ranganatha, S.; Supriya, S.; Ranjan, P.; Chakraborty, T.; Ramakrishna, D. Nickel Curcumin Complexes: Physico Chemical Studies and Nonlinear Optical Activity. *Opt. Mater.* **2023**, *136*, 113450.
(20) Ramakrishna, D.; Bhat, B. R. A catalytic process for the selective oxidation of alcohols by copper (II) complexes. *Inorg. Chem. Commun.* **2011**, *14*, 690−693.
(21) Ramakrishna, D.; Badekai, R. B. Ruthenium Green Conversion of Alcohols to Carbonyls Catalyzed by Novel Ruthenium-Schiff base-triphenylphosphine complexes. *Inorg. Chem. Commun.* **2011**, *14*, 155−158.
(22) Dileep, R.; Badekai, R. B. Palladium-Schiff base-triphenylphosphine catalyzed oxidation of alcohols. *Appl. Organomet. Chem.* **2010**, *24*, 663−666.
(23) Ramakrishna, D.; Bhat, B. R.; Karvembu, R.; Ramasamy, K. Catalytic oxidation of alcohols by nickel (II) Schiff base complexes containing triphenylphosphine in ionic liquid: An attempt towards green oxidation process. *Catal. Commun.* **2010**, *11*, 498−501.
(24) Basappa Chidananda, V. K.; Dileep, R.; Manpreet, K.; Revanasiddappa, H. D. Benzimidazolyl based Schiff-base palladium complex in ionic liquid: An effective combination for Suzuki coupling. *J. Coord. Chem.* **2011**, *70*, 1573−1584.
(25) Pavithra, M. K.; Venkatesha, T. V.; Punith Kumar, M. K.; Manjunatha, K. Investigation of the Inhibition Effect of Ibuprofen Triazole against Mild Steel Corrosion in an Acidic Environment. *Res. Chem. Intermed.* **2015**, *41* (10), 7163−7177.
(26) Pavithra, M. K.; Venkatesha, T. V.; Punith, K. M. K. Inhibiting Effects of Rabeprazole Sulfide on the Corrosion of Mild Steel in Acidic Chloride Solution. *Int. J. Electrochem.* **2013**, *2013*, 714372.
(27) Pavithra, M. K.; Venkatesha, T. V.; Punith Kumar, M. K.; Anantha, N. S. Electrochemical, Gravimetric and Quantum Chemical Analysis of Mild Steel Corrosion Inhibition by Colchicine in 1 M HCl Medium. *Res. Chem. Intermed.* **2016**, *42* (3), 2409−2428.
(28) Prasanna, B. M.; Praveen, B. M.; Narayan, H.; Pavithra, M. K.; Manjunatha, T. S.; Malladi, R. S. Theoretical and experimental approach of inhibition effect by sulfamethoxazole on mild steel corrosion in 1-M HCl. *Surf. Interface Anal.* **2018**, *50*, 779.
(29) Borsari, M.; Ferrari, E.; Grandi, R.; Saladini, M. Curcuminoids as potential new ironchelating agents: spectroscopic, polarographic and potentiometric study on their Fe (III) complexing ability. *Inorg. Chim. Acta* **2002**, *328*, 61−68.
(30) Nandiyanto, A. B. D.; Wiryani, A. S.; Rusli, A.; Purnamasari, A.; Abdullah, A. G.; Widiaty, I.; Widiaty, I.; Hurriyati, R. Extraction of curcumin pigment from Indonesian local turmeric with its infrared spectra and thermal decomposition properties. *IOP Conf. Ser.: Mater. Sci. Eng.* **2017**, *180* (1), 012136.
(31) Zhao, R.; Tan, T.; Sandstrom, C. NMR studies on puerarin and its interaction with beta-cyclodextrin. *J. Biol. Phys.* **2011**, *37*, 387−400.
(32) Valand, N. N.; Patel, M. B.; Menon, S. K. Curcumin-p-sulfonatocalix[4]resorcinarene (p-SC[4]R) interaction: thermo-physico chemistry, stability and biological evaluation. *RSC Adv.* **2015**, *5*, 8739−8752.
(33) Firdhouse, M. J.; Nalini, D. Corrosion Inhibition of Mild Steel in Acidic Media by 5′-Phenyl-2′,4′-dihydrospiro[indole-3,3′-pyrazol]-2(1H)-one. *J. Chem.* **2013**, *9*, 835365.
(34) Lebrini, M.; Robert, F.; Vezin, H.; Roos, C. Electrochemical and quantum chemical studies of some indole derivatives as corrosion inhibitors for C38 steel in molar hydrochloric acid. *Corros. Sci.* **2010**, *52*, 3367−3376.
(35) Lebrini, M.; Robert, F.; Blandinières, P.; Roos, C. Corrosion Inhibition by *Isertia coccinea* Plant Extract in Hydrochloric Acid Solution. *Int. J. Electrochem. Sci.* **2011**, *6*, 2443−2460.
(36) Liao, Z.; Farrell, J.; Junfeng, N.; Bo, Y.; Yang, Y. Electrochemical oxidation of perfluorobutane sulfonate using boron-doped diamond film electrodes. *J. Appl. Electrochem.* **2020**, *39* (10), 1993−1999.
(37) Senhaji, B.; Hmamou, D. B.; Salghi, R.; Zarrouk, A.; Chebli, B.; Zarrok, H.; Warad, I.; Hammouti, B.; Al-Deyab, S. S. *Asteriscus Imbricatus* Extracts: Antifungal Activity and Anticorrosion Inhibition. *Int. J. Electrochem. Sci.* **2013**, *8*, 6033−6046.
(38) Kuruvilla, M.; John, S.; Joseph, A. Electrochemical studies on the interaction of L-cysteine with metallic copper in sulfuric acid. *Res. Chem. Intermed.* **2012**, *39*, 3531−3543.
(39) Pavithra, M. K.; Venkatesha, T. V.; Punith Kumar, M. K.; Tondan, H. C. Inhibition of mild steel corrosion by Rabeprazole sulfide. *Corros. Sci.* **2012**, *60*, 104−111.
(40) Pavithra, M. K.; Venkatesha, T. V.; Vathsala, K.; Nayana, K. O. Synergistic effect of halide ions on improving corrosion inhibition

https://doi.org/10.1021/acsomega.3c10048
ACS Omega 2024, 9, 13262−13273

behaviour of benzisothiozole-3-piperizine hydrochloride on mild steel in 0.5 M H_2SO_4 medium. *Corros. Sci.* **2010**, *52* (11), 3811−3819.
(41) Quraishi, M. A.; Rafiquee, M. Z. A.; Khan, S.; Saxena, N. Corrosion inhibition of aluminium in acid solutions by some imidazoline derivatives. *J. Appl. Electrochem.* **2007**, *37*, 1153−1162.
(42) Gopi, D.; Govindaraju, K. M.; Kavitha, L. Investigation of triazole derived Schiff bases as corrosion inhibitors for mild steel in hydrochloric acid medium. *J. Appl. Electrochem.* **2010**, *40*, 1349−1356.
(43) Laamari, R.; Benzakour, J.; Berrekhis, F.; Abouelfida, A.; Derja, A.; Villemin, D. Corrosion inhibition of carbon steel in hydrochloric acid 0.5 M by hexa methylene diamine tetramethyl-phosphonic acid. *Arab. J. Chem.* **2011**, *4* (3), 271−277.
(44) Ostovari, A.; Hoseinieh, S. M.; Peikari, M.; Shadizadeh, S. R.; Hashemi, S. J. Corrosion inhibition of mild steel in 1 M HCl solution by henna extract: A comparative study of the inhibition by henna and its constituents (Lawsone, Gallic acid, a-D-Glucose and Tannic acid). *Corros. Sci.* **2009**, *51*, 1935−1949.
(45) Noor, E. A. Potential of aqueous extract of Hibiscus sabdariffa leaves for inhibiting the corrosion of aluminum in alkaline solutions. *J. Appl. Electrochem.* **2009**, *39*, 1465−1475.
(46) Hosseini, M. G.; Khalilpur, H.; Ershad, S.; Saghatforoush, L. Protection of mild steel corrosion with new thia-derivative Salens in 0.5 M H_2SO_4 solution. *J. Appl. Electrochem.* **2010**, *40* (2), 215−223.
(47) Mu, G.; Li, X.; Liu, G. Synergistic inhibition between tween 60 and NaCl on the corrosion of cold rolled steel in 0.5 M sulfuric acid. *Corros. Sci.* **2005**, *47* (8), 1932−1952.
(48) Aslam, J.; Aslam, R.; Lone, I. H.; Radwan, N. R.; Mobin, M.; Aslam, A.; Parveen, M.; Al-Freedi, A. A.; Alzulaibani, A. A. Inhibitory effect of 2-Nitroacridone on corrosion of low carbon steel in 1 M HCl solution: An experimental and theoretical approach. *J. Mater. Res. Technol.* **2020**, *9* (3), 4061−4075.
(49) Nataraja, S. E.; Venkatesha, T. V.; Manjunatha, K.; Poojary, B.; Pavithra, M. K.; Tandon, H. C. Inhibition of the Corrosion of Steel in Hydrochloric Acid Solution by Some Organic Molecules Containing the Methylthiophenyl Moiety. *Corros. Sci.* **2011**, *53* (8), 2651−2659.
(50) El-Ferjani, R. M.; Musa, A.; Harun, F. W.; Bulgasem, Y. Synthesis, Characterization and Antibacterial Activity of Schiff Bases Derived from 4-Dimethylaminobenzaldehyde with Some Amino Acids and 4-Aminoantipyrine toward Cu (II), Ni (II), Co(II), Cd (II) and Mn (II) Ions. *IOSR J. Appl. Chem.* **2017**, *10*, 6.
(51) Jayalakshmi, R.; Jayakkumar, V.; Dhivya Priya, D. Synthesis and Characterization of 4-Amino Antipyrine Based Schiff Base Complexes: Antimicrobial, Cytotoxicity and DNA Cleavage Studies. *Int. J. Eng. Res. Sci. Technol.* **2017**, *6* (6), 1.
(52) Jamil, D. M.; Al-Okbi, A. K.; Al-Baghdadi, S. B.; Al-Amiery, A. A.; Abdulhadi, K.; Tayser, S. G.; Abdul, A. H.; Abu, B. M. Experimental and theoretical studies of Schif bases as corrosion inhibitors. *Chem. Cent. J.* **2018**, *12*, 7.
(53) Kuddushi, M. M. Y.; Malek, M. A. H.; Patel, V. L. P. M. S.; Patel, R. K.; Dave, R. H. synthesis and characterization of schiff base aniline with 5-bromo −2- hydroxyl benzaldehyde and their metal complexes. *Int. J. Recent Sci. Res.* **2018**, *9* (4), 26026−26030.
(54) Elemike, E. E.; Onwudiwe, D. C.; Nwankwo, H. U.; Hosten, E. C. Synthesis, crystal structure, electrochemical and anti-corrosion studies of Schiff base derived from o-toluidine and o-chlorobenzaldehyde. *Mol. Struct.* **2017**, *1136* (36), 253−262.
(55) Verma, C.; Quraishi, M. A. Recent progresses in Schiff bases as aqueous phase corrosion inhibitors: Design and applications. *Des. Appl.* **2021**, *446* (446), 214105.
(56) Mahdi, B. S.; Aljibori, H. S. S.; Abbass, M. K.; Al-Azzawi, W.; Kadhum, A. H.; Hanoon, M. M.; Isahak, W. N. R. W.; Al-Amiery, A. A.; Majdi, H. Sh. Gravimetric analysis and quantum chemical assessment of 4-aminoantipyrine derivatives as corrosion inhibitors. *Int. J. Corros. Scale Inhib.* **2022**, *3* (11), 1191−1213.
(57) Ashwini, N.; Dileep, R.; Ranganatha, S. Curcumin and Curcumin Derivatives as Green Corrosion Inhabitor-A Review. *Phys. Chem. Res.* **2023**, *4* (11), 825−835.
(58) Shakeel Nawaz, S.; Manjunatha, K. B.; Supriya, S.; Ranganatha, S.; Ranjan, P.; Chakraborty, T.; Bhat, R.; Ramakrishna, D. Zinc-curcumin complexes: Design, synthesis, geometry optimization, and optical nonlinearity applications. *Opt. Mater.* **2023**, *143*, 114164.
(59) Lgaz, H.; Saha, S. K.; Chaouiki, A.; Bhat, K. S.; Salghi, R.; Shubhalaxmi, P.; Banerjee, P.; Ali, I. H.; Khan, M. I.; Chung, I. M. Exploring the potential role of pyrazoline derivatives in corrosion inhibition of mild steel in hydrochloric acid solution: Insights from experimental and computational studies. *Constr. Build. Mater.* **2020**, *233*, 117320.
(60) Saraswat, V.; Yadav, M.; Obot, I. B. Investigations on eco-friendly corrosion inhibitors for mild steel in acid environment: Electrochemical, DFT and Monte Carlo Simulation approach. *Colloids Surf., A* **2020**, *599*, 124881.

https://doi.org/10.1021/acsomega.3c10048
ACS Omega 2024, 9, 13262−13273